

Surface Reconstruction of Halide Perovskites during Post-treatment

Shaun Tan,^{1,2,‡} Tianyi Huang,^{1,2,‡} Ilhan Yavuz,^{3,‡} Rui Wang,¹ Marc H. Weber,⁴ Yepin Zhao,¹ Maged Abdelsamie,⁵ Michael E. Liao,¹ Hao-Cheng Wang,⁶ Kenny Huynh,¹ Kung-Hwa Wei,⁶ Jingjing Xue,¹ Finn Babbe,² Mark S. Goorsky,¹ Jin-Wook Lee,^{7,*} Carolin M. Sutter-Fella,^{2,8,*} and Yang Yang^{1,*}

¹Department of Materials Science and Engineering and California NanoSystems Institute, University of California Los Angeles, Los Angeles, California 90095, United States.

²Chemical Sciences Division, Lawrence Berkeley National Laboratory, Berkeley, California 94720, United States.

³Department of Physics, Marmara University, 34722, Ziverbey, Istanbul, Turkey.

⁴Center for Materials Research, Washington State University, Pullman, WA 99164, United States.

⁵Materials Science Division, Lawrence Berkeley National Laboratory, Berkeley, California 94720, United States.

⁶Department of Materials Science and Engineering, National Yang Ming Chiao Tung University, Hsinchu 30010, Taiwan

⁷SKKU Advanced Institute of Nanotechnology (SAINT) and Department of Nanoengineering, Sungkyunkwan University, Suwon 16419, Republic of Korea.

⁸Molecular Foundry, Lawrence Berkeley National Laboratory, Berkeley, California 94720, United States.

‡These authors contributed equally to this work.

*Correspondence to:

Y. Yang, email: yangy@ucla.edu

C. M. Sutter-Fella, email: csutterfella@lbl.gov

J.-W. Lee, email: jw.lee@skku.edu

24 **ABSTRACT**

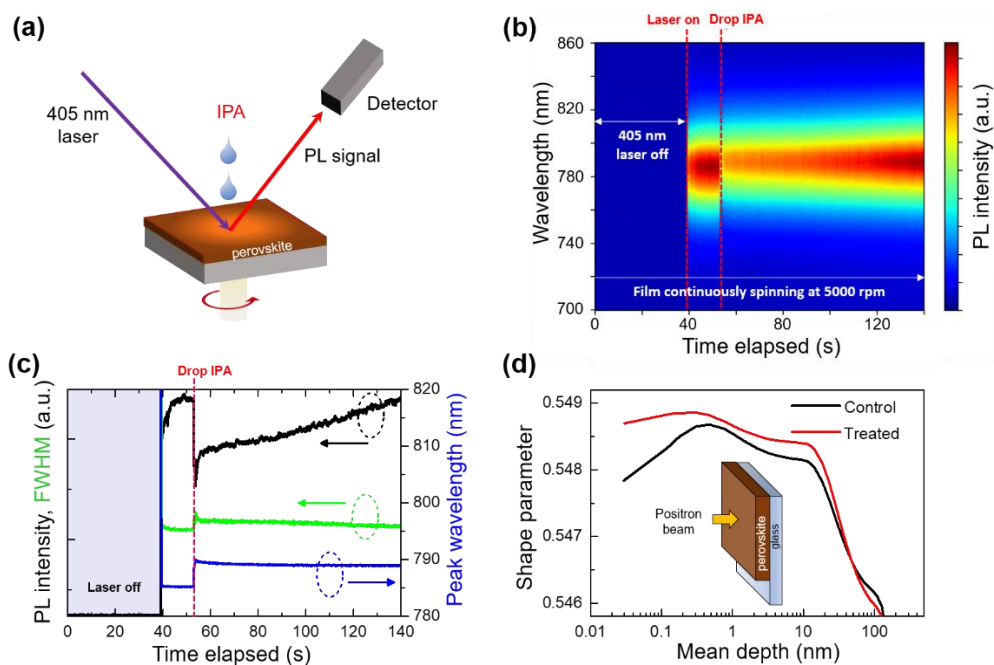
25 Post-fabrication surface treatment strategies have been instrumental to the stability and performance
26 improvements of halide perovskite photovoltaics in recent years. However, consensus understanding of
27 the complex reconstruction processes occurring at the surface is still lacking. Here, we combined
28 complementary surface-sensitive and depth-resolved techniques to investigate the mechanistic
29 reconstruction of the perovskite surface at the microscale level. We observed a reconstruction towards a
30 more PbI_2 -rich top surface induced by the commonly used solvent isopropyl alcohol (IPA). We discuss
31 several implications of this reconstruction on the surface thermodynamics and energetics. Particularly,
32 our observations suggest that IPA assists in the adsorption process of organic ammonium salts to the
33 surface to enhance their defect passivation effects.

34 The record performance of single-junction halide perovskite solar cells (PSCs) have now exceeded
35 25 %.¹ Important breakthroughs on defect passivation strategies have contributed to the rapid performance
36 improvements in recent years.^{2,3} However, achievable voltage losses are still short of the theoretical limit.
37 More importantly, it has become apparent that the migration and redistribution of charged point defects
38 by a potential gradient is known to underly the operational instability of PSCs,⁴⁻⁶ and this remains one of
39 the major challenges of perovskite photovoltaics.

40 It has been reported that defect states causing non-radiative losses are dominantly located towards
41 the top surface of halide perovskites.^{7,8} This has motivated the development of surface passivation
42 strategies by post-treatment of the perovskite film surface.⁹ However, understanding of the complex
43 reconstruction processes that can occur during the surface treatment procedures and any resulting changes
44 to the interfacial charge dynamics are still lacking. This is urgently needed for targeted surface treatment
45 strategies to minimize trial-and-error approaches. For this purpose, *in situ* spectroscopy is suited to
46 monitor occurring changes on relevant time and length scales.¹⁰⁻¹³

47 In this study, we investigate the mechanistic reconstruction processes occurring at the perovskite
48 surface during post-fabrication treatments. Through complementary surface-sensitive techniques, we
49 observed the generation of defects and a reconstruction towards a more PbI₂-rich surface as isopropyl
50 alcohol (IPA) is spun onto the surface. We show that this reconstruction has important implications on the
51 thermodynamics and energetics of the perovskite surface. Importantly, our observations suggest that IPA
52 assists in the anchoring process of organic ammonium salts to the perovskite surface.

53 IPA is ubiquitously used as the solvent to dissolve organic ammoniums for surface treatments, but
54 formamidinium iodide (FAI), itself with the amidinium functional group, is also soluble in IPA. It is
55 unclear what effects (if any) IPA has on the perovskite surface, given the short exposure timescales (~ms)
56 at high rotation speeds (>4000 rpm). Conflicting results on the macroscopic bulk device/film properties
57 have been reported. Beneficial improvements to film crystallinity, charge carrier dynamics, morphology,
58 and device performance have been observed,^{14,15} while detrimental effects to device stability were also
59 reported.¹⁶ To rationalize these contradictory results, we first attempted to explore the microscale
60 phenomena occurring at the surface. Significantly, IPA remains perhaps a crucial solvent for post-
61 treatment, since the most common surface passivating agents, such as phenylethylammonium iodide
62 (PEAI) and octylammonium iodide (OAI), are essentially insoluble in low polarity solvents such as
63 chloroform (CF) (**Figure S1**).



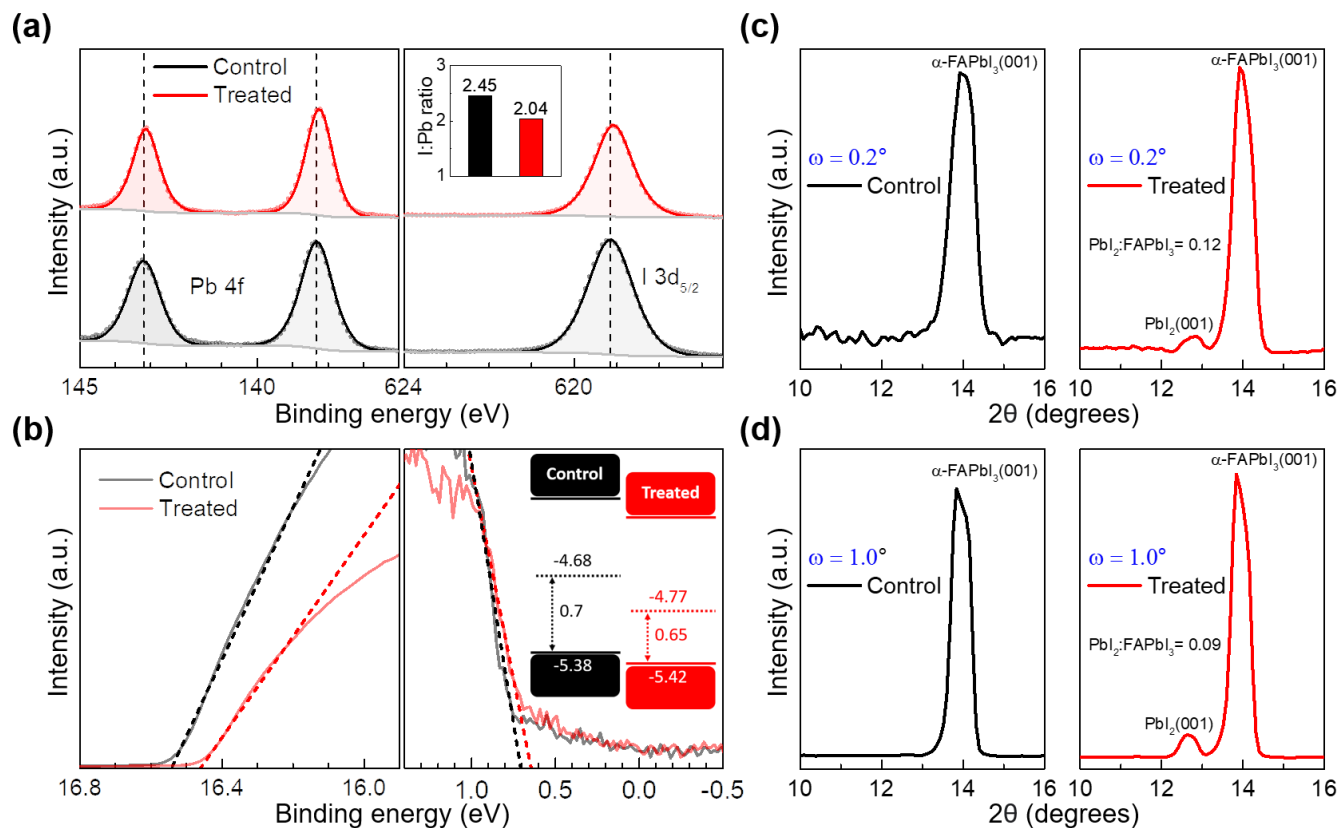
64

65 **Figure 1. Defect generation by IPA treatment.** (a) Schematic of the *in situ* PL measurement during IPA
 66 post-treatment. (b) *In situ* PL contour plot of a perovskite film undergoing surface treatment with IPA
 67 dropped at around 53 s. (c) Evolution of the PL parameters extracted from fitting (b). (d) PAS depth-
 68 profiling of the perovskite films.

69 The control perovskite is based on a FAPbI_3 composition with 5 mol% of added MAPbBr_3
 70 fabricated by a one-step antisolvent quenching method. We monitored the photoluminescence (PL) of an
 71 as-fabricated perovskite film *in situ* with a 405 nm excitation wavelength (**Figure 1a**) in a nitrogen
 72 glovebox (<0.5 ppm $\text{O}_2/\text{H}_2\text{O}$). The laser penetration depth was estimated to be ~ 50 nm (**Figure S2**), and
 73 therefore sensitive to any potential changes in the surface charge carrier recombination behavior. The PL
 74 intensity abruptly decreased (23 % decrease) with a broadening and redshifting of the PL peak upon
 75 dropping IPA (**Figure 1b, 1c, Figure S3a**). In general, this is indicative of increased nonradiative carrier
 76 recombination, which implies the generation of charge-trapping defect states. Time-resolved PL (**Figure**
 77 **S3b**) of the perovskite films further support this, where the carrier lifetime fitted with a mono-exponential
 78 decay function decreased from 1,021 to 793 ns for the control and IPA treated films, respectively. The PL
 79 intensity (and FWHM) is observed to gradually recover with time, possibly due to trap-filling by photo-
 80 generated carriers,¹⁷ as also seen in the control film without treatment (**Figure S3c, 3d**).

81 We further investigated the distribution and nature of the generated defects using Positron
 82 Annihilation Spectroscopy (PAS). Positrons are implanted from the film surface and annihilate with

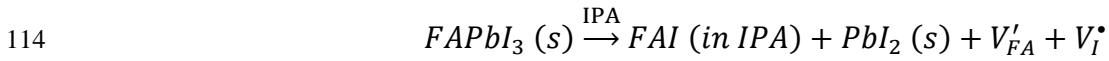
83 electrons after trapping at negatively charged (or neutral) defects to emit two gamma photons. The incident
 84 kinetic energy is controlled to vary the positron implantation depth (**Figure 1d, Figure S4**), from which
 85 the depth-resolved defect density of the film can be investigated. The treated film had a higher Shape
 86 parameter within ~40 nm from the film surface, implying the generation of negatively charged (or neutral)
 87 defects at the top surface region. We speculate that the formed defect is possibly FA vacancy (V_{FA}'), given
 88 the solubility of FAI in IPA.



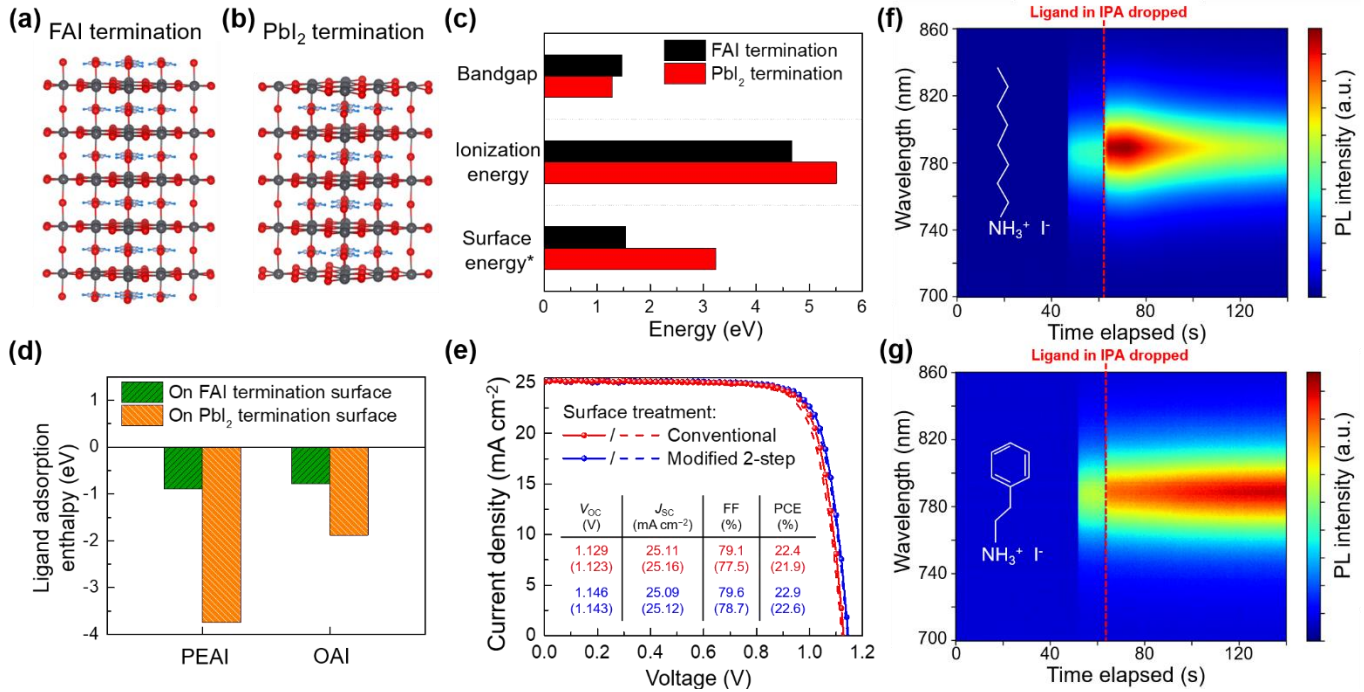
89
 90 **Fig. 2. Characterizations of the perovskite films.** (a) High-resolution XPS spectra of the Pb 4f and I
 91 3d_{5/2} peaks of the perovskite films. Inset includes the calculated I:Pb ratios of the films. Solid lines are
 92 fitted plots. Dashed vertical lines demarcate the peak positions for the control film. Intensities are
 93 normalized to Pb 4f peak. (b) UPS spectra of the perovskite films. Inset includes a schematic band
 94 diagram of the energy levels based on the UPS measurements. GIXRD diffraction patterns of the
 95 perovskite films measured with an incident angle of (c) $\omega = 0.2^\circ$ and (d) $\omega = 1.0^\circ$.

96 The implied existence of V_{FA}' suggests that iodine vacancy (V_I^\bullet) was likely generated
 97 concurrently, but PAS is unable to ascertain this due to its insensitivity to positively charged defects (i.e.
 98 V_I^\bullet).^{18,19} We therefore further probed the films with high-resolution X-ray Photoelectron Spectroscopy

99 (XPS). The I:Pb ratio, calculated from the integrated areas of the Pb 4f doublet and I 3d_{5/2} peak (**Figure**
100 **2a**), was 2.45 for the control film, and decreased to 2.04 for the treated film to approach that of
101 stoichiometric PbI₂. We note that the ultra-high vacuum environment of the XPS instrument (~10⁻⁷-10⁻⁸
102 torr) may have accelerated the outgassing of the volatile halide,^{20,21} and therefore only relative
103 comparisons would be reliable. Closer inspection of the XPS spectra further showed that all of the Pb
104 4f_{5/2} (143.19 eV to 143.13 eV), Pb 4f_{7/2} (138.32 eV to 138.25 eV), and I 3d_{5/2} (619.15 eV to 619.08 eV)
105 characteristic peaks shifted to lower binding energies for the treated film when compared to the control,
106 suggesting a change in the surface chemical environment. Together with the observed change in the I:Pb
107 ratios, the shift direction and final peak positions is consistent with the formation of PbI₂ for the treated
108 film.²² The existence of PbI₂ was directly detected by Grazing Incidence X-ray Diffraction (XRD) at an
109 incident angle of $\omega = 0.2^\circ$ (penetration depth ~60 nm, see Methods for estimation) (**Figure 2c, 2d**).
110 Moreover, the PbI₂:FAPbI₃ peak intensity ratio was observed to decrease at an incident angle of $\omega = 1.0^\circ$
111 (penetration depth ~310 nm), suggesting that the PbI₂ is located more towards the top perovskite region.
112 Combining the experimental observations together, we thus propose the following reconstruction of the
113 perovskite film surface during post-treatment, by a dissolution reaction process induced by IPA:



115 We now discuss some possible implications of this inferred surface reconstruction. Ultraviolet
116 Photoelectron Spectroscopy (UPS) was used to investigate any band structure changes at the surface. The
117 fermi level was observed to downshift from -4.68 eV for the control film to -4.77 eV for the film treated
118 with IPA (**Figure 2b**), indicating a more p-doped surface for the latter relative to the bare perovskite
119 surface. The overall band structure of the treated surface further downshifted relative to the vacuum level
120 due to the deeper valence band maximum (inset of **Figure 2b**), consistent with a relatively more FAI
121 deficient surface.²³ This possibly creates a more beneficial band bending going from the perovskite bulk
122 to the surface contacting a hole-transporting material (**Figure S5a**). The surface PbI₂ for the treated film
123 may additionally contribute to interfacial passivation.²⁴ In reality, however, we observed that the treated
124 device performance was inferior to the control with a more pronounced current-voltage hysteresis (**Figure**
125 **S5b, S5c**), likely due to the generated vacancy defects, given that defect migration (due to the bias
126 potential) is known to underly the hysteric behavior.^{4,9}



127

128

129

130

131

132

133

134

Figure 3. Surface reconstruction and its implications. (a), (b) Theoretical slab models for first-principles DFT calculations. Atoms are colored black (lead), red (iodine), gray (nitrogen), and blue (hydrogen). (c) Calculated surface physiochemical properties. The asterisk indicates that surface energy is in units of eV nm⁻². (d) Enthalpy of adsorption of either PEAI or OAI on the surfaces. (e) Current density-voltage curves of devices treated with 10 mM OABr in CF. Inset includes the measured photovoltaic parameters. Brackets indicate parameters measured in forward bias. *In situ* PL contour plots of perovskite films undergoing surface treatment with (f) 10 mM OAI or (g) 10 mM PEAI in IPA.

135

136

137

138

139

140

141

142

143

144

145

First-principles density functional theory (DFT) calculations were performed on slabs based on the deduced reconstruction to compare their thermodynamics and energetics. We note that realistically, the perovskite surface is expected to be a complex amalgamation of exposed atoms, local atomic pairing/reorientation, and defected.²⁵ However, simplified slab models are necessarily required to reduce computational complexity. Nevertheless, *relative* comparisons can be made based on the predicted results. Experimental investigations have observed that the pristine perovskite surface (without treatment) is terminated mostly by organic halides,^{26,27} which is also supported by computational results.²⁸ Our results imply that IPA reconstructs the surface towards a *relatively more* PbI₂-rich surface. We chose the two extreme cases of complete FAI termination (**Figure 3a**) and PbI₂ termination (**Figure 3b**) to model the pristine (control) and reconstructed (treated) surfaces, respectively, again noting that the models are used to predict *relative trends*.

146 The predicted bandgap decreased while the ionization energy increased for the PbI_2 termination
147 surface (**Figure 3c**), matching the *in situ* PL and UPS observations discussed. The surface energy more
148 than doubled (1.54 to 3.24 eV nm⁻²) for the PbI_2 termination surface, indicating that the surface became
149 more thermodynamically unstable with treatment. This likely contributed to the observed aggravated
150 instability of the treated films (**Figure S6**). The generated defects might additionally lower the FAPbI_3
151 cubic-to-hexagonal phase transformation activation energy barrier to also accelerate the degradation.²⁹
152 Given the increased surface energy, we postulated that organic ammonium salts may preferentially adsorb
153 onto the treated surface. We further calculated the formation enthalpy to attach the widely used passivation
154 agents OAI or PEAI to the surfaces (**Figure 3d**). The adsorption enthalpies for both were significantly
155 more negative on the PbI_2 termination surface – for OAI, -0.78 versus -1.88 eV (141% increase), and -0.9
156 versus -3.75 eV for PEAI (317% increase), suggesting that the surface reconstruction plays a vital role in
157 the passivation process.

158 The more negative adsorption enthalpies imply that ammonium salts are thermodynamically
159 more favored to adsorb onto the treated surface. We investigated this with a modified 2-step surface
160 post-treatment process (**Figure S7**). Initially treating a perovskite film with pure IPA before
161 subsequently depositing octylammonium bromide (OABr) in CF (at the same concentration) further
162 improved the device photovoltaic performance (**Figure 3e**). The champion device surface treated with
163 the modified 2-step approach reached a power conversion efficiency of 22.9 % in reverse bias (**Figure**
164 **3e**) with negligible current-voltage hysteresis, relative to the 22.4 % of the conventionally treated
165 device. The improved performance was attributed to increases in the device open-circuit voltage (1.129
166 V to 1.146 V) and fill factor (79.1 % to 79.6 %), which is indicative of an enhanced defect passivation
167 effect with the modified 2-step treatment. Therefore, the observations support the theoretical predictions
168 that IPA assists in the adsorption process of ammonium salts to the surface and thus the passivation of
169 defects. The surface is first reconstructed by removing FAI to expose the undercoordinated Pb^{2+} (i.e. V_l^*)
170 for the ammonium groups to bond with by electrostatic coulomb interactions and/or hydrogen bonding.

171 We speculated that the PL evolution as OAI or PEAI (in IPA) is deposited on the surface may be
172 related to their adsorption enthalpies. Further measurements show that although both treatments led to
173 instantaneous PL enhancements immediately upon deposition (**Figure 3f, 3g, Figure S8**), the PL
174 intensity subsequently decayed ~10 s after deposition only for the OAI treated film. With the PbI_2
175 termination surface, the computed adsorption enthalpies imply a significantly weaker interaction of OAI
176 (relative to PEAI) with the perovskite surface, which may possibly be correlated with the differing PL

177 dynamics. On the other hand, the adsorption enthalpies are negligibly different when calculated using
178 the FAI termination surface, which may be challenging to reconcile with the experimental observation.
179 We also monitored the recombination dynamics with further *in situ* PL measurements during annealing
180 (**Figure S9a, S9b**). A rapid initial exponential decay in PL intensity was observed for both films due to
181 increased phonon scattering at elevated temperatures.^{10,12} However, only the OAI treated film
182 counteracted the initial drop to eventually increase its PL intensity due to the activated defect
183 passivation effect. The evolution and emission characteristics of the wide bandgap phases notably differ
184 between the OAI and PEAI treated films, and will be the subject of future investigations (**Figure S9c,**
185 **S9d, S9e**).

186 In summary, we observed a reconstruction of the perovskite top surface induced by IPA, which
187 is ubiquitously used as the solvent for surface treatment with organic ammonium salts. We discussed
188 several implications of this reconstruction on the perovskite surface energetics and thermodynamics.
189 Importantly, given the profound differences between the reconstructed surface and the perovskite
190 bulk/pristine surface, these results will guide further experimental and theoretical investigations of the
191 perovskite surface and surface passivation strategies.

192 ASSOCIATED CONTENT

193 Supporting Information

194 The Supporting Information is available free of charge on the ACS Publications website at DOI: XXX

195

196 Materials and methods; Photographs of ammonium salts in CF; PL penetration depth estimation; *In situ*
197 and time-resolved PL spectra of the perovskite films; PAS profile of the perovskite films; Device energy
198 alignment and performance; Humidity stability testing on the perovskite films; Modified surface treatment
199 process; *In situ* PL of films undergoing surface treatment; *In situ* PL of films undergoing post-annealing.
200 (PDF)

201 AUTHOR INFORMATION

202 Corresponding Authors

203 **Jin-Wook Lee** – *SKKU Advanced Institute of Nanotechnology (SAINT) and Department of*
204 *Nanoengineering, Sungkyunkwan University, Suwon 16419, Republic of Korea;*
205 Email: jw.lee@skku.edu

206 **Carolyn M. Sutter-Fella** – *Chemical Sciences Division and Molecular Foundry, Lawrence*
207 *Berkeley National Laboratory, Berkeley, California 94720, United States;*
208 Email: csutterfella@lbl.gov

209 **Yang Yang** – *Department of Materials Science and Engineering and California NanoSystems*
210 *Institute, University of California Los Angeles, Los Angeles, California 90095, United States;*
211 Email: yangy@ucla.edu

212 **Author Contributions**

213 ‡These authors contributed equally.

214 **Notes**

215 The authors declare no competing financial interests.

216 **ACKNOWLEDGMENT**

217 This work was supported by the U.S. Department of Energy’s Office of Energy Efficiency and Renewable
218 Energy (EERE) under the Solar Energy Technologies Office under award number DE-EE0008751. Dr.
219 Carolin M. Sutter-Fella acknowledges the Molecular Foundry supported by the Department of Energy,
220 Office of Science, Office of Basic Energy Sciences, Scientific User Facilities Division of the U.S.
221 Department of Energy under contract no. DE-AC02-05CH11231. Dr. Marc H. Weber would like to
222 acknowledge the detailed discussions with the late Kelvin G. Lynn. Dr. Marc H. Weber’s contributions
223 and the positron annihilation spectroscopy work was supported by subcontract to Washington State
224 University from the University of California, Los Angeles of a grant by the U.S. Department of Energy’s
225 Office of Energy Efficiency and Renewable Energy (EERE) under the Solar Energy Technologies Office
226 under award number DE-EE0008751 awarded to Dr. Yang Yang. Computing resources used in this work
227 were provided by the National Center for High-Performance Computing of Turkey (UHEM) with grant
228 number 1008342020. Dr. Ilhan Yavuz acknowledges support by the Scientific and Technological Research
229 Council of Turkey (TÜBİTAK), Grant no: 119F380. Dr. Jin-Wook Lee acknowledges support by the
230 National Research Foundation of Korea (NRF) grant funded by the Korea government (MIST) under
231 contract number NRF-2020R1F1A1067223. Shaun Tan, Tianyi Huang, Dr. Maged Abdelsamie, Dr. Finn
232 Babbe, and Dr. Carolin M. Sutter-Fella acknowledge support from the Laboratory Directed Research and
233 Development (LDRD) program of Lawrence Berkeley National Laboratory under U.S. Department of
234 Energy contract number DE-AC02-05CH11231.

235 **References**

- 236 1. Best Research-Cell Efficiency Chart (2020). NREL.
- 237 2. Jiang, Q., Zhao, Y., Zhang, X., Yang, X., Chen, Y., Chu, Z., Ye, Q., Li, X., Yin, Z., and You, J.
238 (2019). Surface passivation of perovskite film for efficient solar cells. *Nat. Photonics* *13*, 460–
239 466.

- 240 3. Kim, G., Min, H., Lee, K.S., Lee, D.Y., Yoon, S.M., and Seok, S. Il (2020). Impact of strain
241 relaxation on performance of α -formamidinium lead iodide perovskite solar cells. *Science* 370,
242 108–112.
- 243 4. Tan, S., Yavuz, I., De Marco, N., Huang, T., Lee, S., Choi, C.S., Wang, M., Nuryyeva, S., Wang,
244 R., Zhao, Y., et al. (2020). Steric Impediment of Ion Migration Contributes to Improved
245 Operational Stability of Perovskite Solar Cells. *Adv. Mater.* 32, 1906995.
- 246 5. Ball, J.M., and Petrozza, A. (2016). Defects in perovskite-halides and their effects in solar cells.
247 *Nat. Energy* 1, 1–13.
- 248 6. Lee, J.-W., Kim, S.-G., Yang, J.-M., Yang, Y., and Park, N.-G. (2019). Verification and
249 mitigation of ion migration in perovskite solar cells. *APL Mater.* 7, 1–12.
- 250 7. Ni, Z., Bao, C., Liu, Y., Jiang, Q., Wu, W.-Q., Chen, S., Dai, X., Chen, B., Hartweg, B., Yu, Z., et
251 al. (2020). Resolving spatial and energetic distributions of trap states in metal halide perovskite
252 solar cells. *Science* 367, 1352–1358.
- 253 8. Yang, Y., Yang, M., Moore, D.T., Yan, Y., Miller, E.M., Zhu, K., and Beard, M.C. (2017). Top
254 and bottom surfaces limit carrier lifetime in lead iodide perovskite film. *Nat. Energy* 2, 1–7.
- 255 9. Han, T.-H., Tan, S., Xue, J., Meng, L., Lee, J.-W., and Yang, Y. (2019). Interface and Defect
256 Engineering for Metal Halide Perovskite Optoelectronic Devices. *Adv. Mater.* 31, 1803515.
- 257 10. Babbe, F., and Sutter-Fella, C.M. (2020). Optical Absorption-Based In Situ Characterization of
258 Halide Perovskites. *Adv. Energy Mater.* 10, 1903587.
- 259 11. Song, T.-B., Yuan, Z., Babbe, F., Nenon, D.P., Aydin, E., De Wolf, S., and Sutter-Fella, C.M.
260 (2020). Dynamics of Antisolvent Processed Hybrid Metal Halide Perovskites Studied by In Situ
261 Photoluminescence and Its Influence on Optoelectronic Properties. *ACS Appl. Energy Mater.* 3,
262 2386–2393.
- 263 12. Song, T., Yuan, Z., Mori, M., Motiwala, F., Segev, G., Masquelier, E., Stan, C. V., Slack, J.L.,
264 Tamura, N., and Sutter-Fella, C.M. (2020). Revealing the Dynamics of Hybrid Metal Halide
265 Perovskite Formation via Multimodal In Situ Probes. *Adv. Funct. Mater.* 30, 1908337.
- 266 13. Lee, J.-W., Tan, S., Han, T.-H., Wang, R., Zhang, L., Park, C., Yoon, M., Choi, C., Xu, M., Liao,
267 M.E., et al. (2020). Solid-phase hetero epitaxial growth of α -phase formamidinium perovskite.
268 *Nat. Commun.* 11, 5514.
- 269 14. Prochowicz, D., Tavakoli, M.M., Solanki, A., Goh, T.W., Pandey, K., Sum, T.C., Saliba, M., and
270 Yadav, P. (2018). Understanding the effect of chlorobenzene and isopropanol anti-solvent

- 271 treatments on the recombination and interfacial charge accumulation in efficient planar perovskite
272 solar cells. *J. Mater. Chem. A* 6, 14307–14314.
- 273 15. Wang, X., Li, X., Tang, G., Zhao, L., Zhang, W., Jiu, T., and Fang, J. (2015). Improving
274 efficiency of planar hybrid CH₃NH₃PbI₃-xCl_x perovskite solar cells by isopropanol solvent
275 treatment. *Org. Electron.* 24, 205–211.
- 276 16. Yoo, J.J., Wieghold, S., Sponseller, M.C., Chua, M.R., Bertram, S.N., Putri, T., Tresback, J.S.,
277 Hansen, E.C., Correa-Baena, J.-P., Bulović, V., et al. (2019). An interface stabilized perovskite
278 solar cell with high stabilized efficiency and low voltage loss. *Energy Environ. Sci.* 12, 2192–
279 2199.
- 280 17. DeQuilettes, D.W., Zhang, W., Burlakov, V.M., Graham, D.J., Leijtens, T., Osherov, A., Bulović,
281 V., Snaith, H.J., Ginger, D.S., and Stranks, S.D. (2016). Photo-induced halide redistribution in
282 organic–inorganic perovskite film. *Nat. Commun.* 7, 1–9.
- 283 18. Barthe, M.-F., Labrim, H., Gentils, A., Desgardin, P., Corbel, C., Esnouf, S., and Piron, J.P.
284 (2007). Positron annihilation characteristics in UO₂: for lattice and vacancy defects induced by
285 electron irradiation. *Phys. Status Solidi C* 10, 3627–3632.
- 286 19. Wiktor, J., Jomard, G., Torrent, M., and Bertolus, M. (2017). First-principles calculations of
287 momentum distributions of annihilating electron–positron pairs in defects in UO₂. *J. Phys.*
288 *Condens. Matter* 29, 1–9.
- 289 20. Jiang, Y., Yang, S.-C., Jeangros, Q., Pisoni, S., Moser, T., Buecheler, S., Tiwari, A.N., and Fu, F.
290 (2020). Mitigation of Vacuum and Illumination-Induced Degradation in Perovskite Solar Cells by
291 Structure Engineering. *Joule* 4, 1087–1103.
- 292 21. Das, C., Wussler, M., Hellmann, T., Mayer, T., and Jaegermann, W. (2018). In situ XPS study of
293 the surface chemistry of MAPi solar cells under operating conditions in vacuum. *Phys. Chem.*
294 *Chem. Phys.* 20, 17180–17187.
- 295 22. Juarez-Perez, E.J., Ono, L.K., Maeda, M., Jiang, Y., Hawash, Z., and Qi, Y. (2018).
296 Photodecomposition and thermal decomposition in methylammonium halide lead perovskites and
297 inferred design principles to increase photovoltaic device stability. *J. Mater. Chem. A* 6, 9604–
298 9612.
- 299 23. Meggiolaro, D., Mosconi, E., Proppe, A.H., Quintero-Bermudez, R., Kelley, S.O., Sargent, E.H.,
300 and De Angelis, F. (2019). Energy Level Tuning at the MAPbI₃ Perovskite/Contact Interface
301 Using Chemical Treatment. *ACS Energy Lett.* 4, 2181–2184.

- 302 24. Chen, Q., Zhou, H., Song, T. Bin, Luo, S., Hong, Z., Duan, H.S., Dou, L., Liu, Y., and Yang, Y.
303 (2014). Controllable self-induced passivation of hybrid lead iodide perovskites toward high
304 performance solar cells. *Nano Lett.* *14*, 4158–4163.
- 305 25. Leblebici, S.Y., Leppert, L., Li, Y., Reyes-Lillo, S.E., Wickenburg, S., Wong, E., Lee, J., Melli,
306 M., Ziegler, D., Angell, D.K., et al. (2016). Facet-dependent photovoltaic efficiency variations in
307 single grains of hybrid halide perovskite. *Nat. Energy* *1*, 1–7.
- 308 26. She, L., Liu, M., and Zhong, D. (2016). Atomic structures of CH₃NH₃PbI₃ (001) surfaces. *ACS*
309 *Nano* *10*, 1126–1131.
- 310 27. Stecker, C., Liu, K., Hieulle, J., Ohmann, R., Liu, Z., Ono, L.K., Wang, G., and Qi, Y. (2019).
311 Surface Defect Dynamics in Organic– Inorganic Hybrid Perovskites: From Mechanism to
312 Interfacial Properties. *ACS Nano* *13*, 12127–12136.
- 313 28. Geng, W., Tong, C.-J., Tang, Z.-K., Yam, C., Zhang, Y.-N., Lau, W.-M., and Liu, L.-M. (2015).
314 Effect of surface composition on electronic properties of methylammonium lead iodide
315 perovskite. *J. Mater.* *1*, 213–220.
- 316 29. Tan, S., Yavuz, I., Weber, M.H., Huang, T., Chen, C.-H., Wang, R., Wang, H.-C., Ko, J.H.,
317 Nuryyeva, S., Xue, J., et al. (2020). Shallow Iodine Defects Accelerate the Degradation of α -
318 Phase Formamidinium Perovskite. *Joule* *4*, 2426–2442.